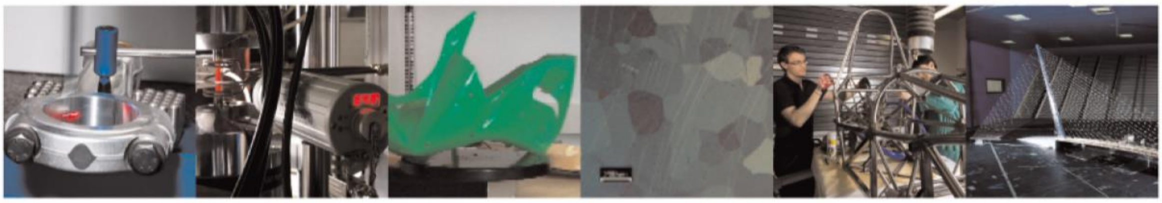

# Cold Microdrawing of Pure Magnesium Capillary Structures for Biomedical Applications

Margherita Pizzi, Francesco De Gaetano, Marco Ferroni, Francesco Arleo, Federica Boschetti, Matteo Strano, Massimiliano Annoni

This is a post-peer-review, pre-copyedit version of an article published in J. Micro Nano-Manuf. Mar 2023, 11(1): 011002, on January 10, 2024. The final authenticated version is available online at: https://doi.org/10.1115/1.4064297

https://asmedigitalcollection.asme.org/micronanomanufacturing/article/11/1/011002/1192777/Cold-Microdrawing-of-Pure-Magnesium-Capillary



DIPARTIMENTO DI MECCANICA ■ POLITECNICO DI MILANO
via G. La Masa, 1 ■ 20156 Milano ■ EMAIL (PEC): pecmecc@cert.polimi.it
http://www.mecc.polimi.it
Rev. 0

# Cold microdrawing of pure magnesium capillary structures for biomedical applications

**Margherita Pizzi**[1]
Department of Mechanical Engineering, Politecnico di Milano 20156 Milan, Italy
Email: margherita.pizzi@polimi.it

**Francesco De Gaetano**
Department of Chemistry, Materials and Chemical Engineering “Giulio Natta”,
Politecnico di Milano 20133 Milan, Italy
Email: francesco.degaetano@polimi.it

**Marco Ferroni**
MgShell S.r.l., 20133 Milan, Italy
Email: marco.ferroni@mgshell.com

**Francesco Arleo**
WatAJet S.r.l., 21010 Varese, Italy
Email: francesco.arleo@watajet.com

**Federica Boschetti**
Department of Chemistry, Materials and Chemical Engineering “Giulio Natta”,
Politecnico di Milano 20133 Milan, Italy
Email: federica.boschetti@polimi.it

**Matteo Strano**
Department of Mechanical Engineering, Politecnico di Milano 20156 Milan, Italy
Email: matteo.strano@polimi.it

**Massimiliano Annoni**
Department of Mechanical Engineering, Politecnico di Milano 20156 Milan, Italy
Email: massimiliano.annoni@polimi.it

[1] Corresponding author

**ABSTRACT**

*This paper presents a study on cold microdrawing of pure magnesium for biomedical applications, where hollow sinking drawing of microtubes of 820 μm diameter and wall thickness around 100 μm was used, varying drawing speeds to achieve a significant reduction in cross-sectional area in a single pass. Results showed an improved surface finish with reduced surface roughness after drawing. The material exhibited an increase in microhardness and ultimate tensile strength by 41% due to work hardening caused by plastic deformation. The study also identified wall thickening of the tube and observed springback behavior of Mg at the die exit. Drawing forces were collected for process monitoring, and finite element (FE) simulations were conducted to assess the risk of pure Mg microtube breakage. This research contributes to advancing the state of the art in Mg microtube drawing, addressing the unique challenge of working with such small tube dimensions where limited studies currently exist.*

***Key words:*** *Microtubes, magnesium, cold drawing, hollow sinking, biomedical devices*

## 1. INTRODUCTION

Magnesium (Mg) and its alloys are widely studied in the field of biomaterials due to their high biocompatibility and low toxicity, being one of the essential components in the regulatory mechanisms of the human body [1, 2]. Their application becomes very interesting when implantable bioresorbable devices are involved, which are supposed to perform their function for a limited period of time inside the body [3]. The best known and largest applications concern cardiovascular stents and bone implants, where the corrosion of the material within the body fluids is exploited in order to allow the device to disappear completely once it is no longer useful, with the great advantage of avoiding removal surgery [4, 5]. Although pure magnesium represents an excellent candidate for the present applications, the most suitable technology for prototyping miniaturized devices needs to be extensively investigated. In fact, Mg is known for its high corrosion rate, poor mechanical properties and poor processability.

Mg tubular products are becoming increasingly more relevant for medical applications such as injection needles, bone-joint implants, and blood-tube stents [6, 7]. Among all the metal forming processes, drawing is widely used for the production of tubular Mg-based components which allows a tube diameter to be significantly reduced using a die. In cold drawing operations, the workpiece predominantly experiences tensile stresses as a result of being pulled through a die. However, a certain degree of compression stress is also imparted to the material as it passes through the die [8]. The maximum reduction in the cross-sectional area achievable for Mg alloys changes depending on whether the process is performed in cold or warm conditions. In the first case the value is around 5% and significantly lower than the 15% achievable under heated conditions [9]. In fact, Mg-based materials are characterized by hexagonal closed-packed (HCP) structure with limited slip systems which causes different issues such as i) poor ductility at room temperature, ii) low finished product yield and iii) high cost of cold drawing tubes. All of these aspects lead to manufacturing difficulties and poor control of surface quality and thickness uniformity [10, 11, 12]. Hot plastic deformation is a widely employed technique with advantageous effects on the metal flow behavior of magnesium alloys. Additionally, it facilitates microstructure refinement through strain accumulation, resulting in uniform deformation and enhanced mechanical properties

[13, 14, 15]. On the other hand, using high temperatures would imply too high production costs. For these reasons, Mg material necessitates the use of numerous cold drawing passes and intermediate annealing phases, as large reductions in cross-sectional area and wall thicknesses cannot be achieved in a single step [9]. Moreover, when dealing with microdiameters and thin walls, size effects related to grain size, friction and difficulties in the manufacture of dies and tools occur, making the process even more challenging. Microforming of such small tubes may induce lower formability, higher risk of failure while drawing and generate more expensive manufacturing processes chains. In fact, to the authors' knowledge, no studies in the scientific literature are related to magnesium capillaries with diameter below 1 mm and thickness as low as 100 microns.

There are several drawing strategies that can be used. The simplest way is called hollow sinking, where the tube is forced to pass through the die, without any internal support used in order to control the thickness. Other techniques, on the other hand, involve the use of a tool held inside the tube that can be fixed (fixed plug tube drawing) or mobile (mandrel drawing and floating plug drawing), as shown in Fig. 1 [10]. In these latter cases, it is also possible to control the thickness of the tube, thanks to the action of the tool from the inside [9].

In this work, a study on the drawing of pure magnesium for thin-walled and fine tubes is presented. In this context, the drawing technique hollow sinking was used to obtain Mg capillaries, hence a considerable reduction in cross-sectional area with a single pass in a die could be obtained. This procedure was selected for this preliminary investigation, to avoid any issue related to the use of a plug or a solid mandrel, according to the study reported by Yoshida et al. [10]. In fact, the study demonstrated the unsuitability of plug drawing, despite being a widely used method for obtaining thin-walled tubes. This method, in fact is poorly suited for magnesium and its alloys due to brittleness. In the same study, the feasibility of drawing with mandrel was evaluated. Again, several problems arose related to the difficulty in extracting the inner mandrel core used. The typical feasible reduction ratios in microdrawing of magnesium tubes ranges between 5 and 15%. In the present paper a reduction ratio larger than 10% is aimed at, using cold sinking with unprecedented small capillary dimensions. Changes in the material mechanical properties were observed in terms of hardness on the cross-sectional surface and by means of tensile test at failure. Moreover, external surface roughness, wall thickening and circularity of the cross-section of drawn tubes were evaluated. Drawing force was also measured as an output of the experiments. Indeed, these data could be useful for process monitoring. To support the experimental results, FE analyses were performed to observe how the drawing speed affects the damage incurred by the tube.

## 2. MATERIAL AND METHODS

### 2.1 Material characterization

Pure Mg material was chosen because of its workability, which is higher than other magnesium alloys for biomedical use, and to avoid issues related to alloying elements that may make the topic of biocompatibility complex [16].

Hence, 99.5% pure magnesium extruded tubes with starting outer diameter $D_{0-out}$ and wall thickness $Th_0$ equal to respectively 829 µm ($\sigma$ = 13.9 µm) and 119 µm ($\sigma$ = 6.95 µm), were used for this experimental study. In order to characterize the as received material, uniaxial tensile tests at failure were carried out on 3 samples using a dynamometer with a ±5 kN static load cell (INSTRON 3366/Q9034, Norwood, Massachusetts, USA) using a loading rate equal to 10 mm/min. The same procedure was carried out on 3 drawn tubes after the experiments to observe the effect of work hardening due to plastic deformation. In this case, the same loading rate was used with a load cell equal to 225 N mounted on a BOSE Enduratec ELF 3200 machine (TA Instruments., New Castle, DE, USA).

Moreover, in order to investigate the effect of plastic deformation due to the drawing process on mechanical properties, the microhardness variation on the cross-section of the microtubes embedded in the cold resin and polished was measured 3 times for each sample with a microhardness tester (FM-810, FUTURE-TECH CORP., Kawasaki, Japan) based on the Vickers hardness with a load of 50 g and a dwell time of 15 s.

The optical microscope LEICA MEF4M (Leica Microsystems, Wetzlar, Germany) was also used to observe the cross-sectional surface pattern of the as received microtube. Hence, after polishing, the sample was chemically etched with Nital 2% to reveal the microstructure. Figure 2 (a) represents a micrograph of the analyzed cross-section. Here, the presence of mechanical twins on the surface produced by the previous states of cold plastic deformation is visible. In this situation, detecting grain boundaries and thus measuring grain size becomes very challenging. From the cross-sections shown in Fig. 2 (a), it can be seen that the starting samples do not have a uniform wall thickness. This characteristic could somehow affect the microtube's ability to withstand the drawing process.

### 2.2 Drawing experimental setup

The hollow sinking cold drawing method was chosen for this experimental study, to obtain a substantial reduction of the cross-section area of the starting Mg microtube in a single pass.

Figure 2 (b) shows a diagram of the proposed hollow sinking drawing process, where the relevant factors influencing the tube's drawability are reported, as the inlet diameters ($D_{0-out}$ and $D_{0-in}$) and outlet diameters ($D_{n-out}$ and $D_{n-in}$) of the tube. These factors determine the total reduction in area $R_{\%}$, according to Eqn. (1) [17]:

$$R_{\%} = \left(1 - \frac{A_n}{A_0}\right) \cdot 100\ [\%] \quad (1)$$

Where $A_0$ and $A_n$ represent the initial and final tube cross-sections, defined according to Eqn. (2) and Eqn. (3), respectively:

$$A_0 = \frac{\pi \cdot (D_{0-out}{}^2 - D_{0-in}{}^2)}{4} \quad (2)$$

$$A_n = \frac{\pi \cdot (D_{n-out}{}^2 - D_{n-in}{}^2)}{4} \quad (3)$$

Figure 2 (b) also shows the geometric characteristics of the diamond-insert die (Balloffett, Lagnieu, France), such as the approach angle $2\alpha$ and the bearing length $L_b$ (see Table 1).

Therefore, a prediction of $R_{\%}$ can be made using Eq. 1 with the starting assumption that the thickness of the tube after drawing is negligible and that $D_{n-out}$ is equal to $D_{die}$, a $R_{\%}$ value equal to 11.34% is obtained. This theoretical value was then compared with that measured downstream of the experiments to quantify any wall thickening. In fact, it has been observed in literature that an increase in small tubes wall thickness can occur during hollow sinking drawing when passes are repeated several times [10].

In this experimental campaign, 6 Mg microtube samples, with initial length $l_{0-sample}$ = 40 mm, were tested by varying the drawing speed $v$ over two levels. The test conditions are reported in Table 2.

This experimental scheme provided 3 replicates for the analysis of the process as a function of the drawing speed $v$. The values of $v$ were selected based on the dynamometer's maximum speed of 500 mm/min. To investigate the impact of velocity on the process, the lower limit was chosen an order of magnitude lower. All the tests were conducted at room temperature with lubrication in order to decrease the drawing force (Hard-Cut 541, Hangsterfers, Mantua Township, USA) and using a dynamometer with a ±5 kN static load cell (INSTRON 3366/Q9034). During drawing, forces were acquired by the load cell. To thread the tube into the die, one of the two ends of the sample was hammered. This commonly used practice, however, resulted in a waste of material.

### 2.3 Surface roughness, tube dimensions and cross-section circularity

As a factor influencing corrosion kinetics, external surface roughness was examined [18]. Surface roughness measurements were made using the 3D microscope Alicona InfiniteFocus G4 (Bruker Alicona, Graz, Austria) to observe how this parameter is affected by the drawing process. For each sample, 3 measurements were made before and after the experiment using the 'SurfaceTextureMeasurement' function in the Alicona software, as shown in Fig. 3 (a). For all the measurements, a cutoff wavelength equal to 800 μm was selected for the 500x200 μm measurement region.

The relevant factor taken into account is the average height of selected area *Sa*.

To assess the homogeneity of the tube's outer diameter after the drawing process, 3 measurements of $D_{0\text{–out}}$ and $D_{n\text{–out}}$ were taken on each sample. The "3DFormMeasurement" module of the Alicona software was used in this case, which allows to obtain the cylinder that best fits the dataset, and thus all the geometric dimensions of the portion of the tube of interest, as shown in Fig. 3 (b). Moreover, the wall thickness was calculated from the difference between the outer diameter of the tube and the inner diameter. The latter was measured using calibrated pins with 0.1 mm pitch (Azuréa Microtechnique SA, Bévilard, Switzerland) before and after the tests.

Circularity of cross-section of the tube was evaluated using the software ImageJ (NIH), from images obtained by the LEICA MEF4M optical microscope.

### 2.4 FE Simulations

Finite element analyses were performed to evaluate process stability and to observe the influence of drawing speed on Mg damage. Forge, an elasto viscoplastic implicit FE simulations software (version 3.0, Transvalor S.A., Biot, France) was used, in which a setup composed by the tube inserted inside the die and drawn by a puller was created, as shown in Fig. 4. For the simulation, a microtube with initially perfect cylindrical geometry (dimensions $D_{0\text{–out}}$ = 820 μm and $Th_0$ = 115 μm) and a die with dimensions reported in Table 1 were used. In the cold drawing simulations, the tube is drawn by a puller that is driven by a hydraulic press with the two drawing speeds used in the experiments (see Table 2). Only 1/8 of the system was simulated, with the assumption of symmetry planes. Then a cold drawing was simulated, thus with a tool and tube temperature of 25°C. The part was modeled using tetrahedral elements, with an average of 4 elements through the thickness of the tube. The drawing die was modeled as perfectly rigid.

The friction Coulomb limited Tresca model was used in order to model the oil friction condition between die and tube. The coefficients $\mu$ and $\bar{\mu}$ were selected during model calibration. It was assumed that the selected velocities for the experiment are not high enough to observe significant effects in terms of tribological behavior, for this reason, the same friction coefficients $\mu$ = 0.025 and $\bar{\mu}$ = 0.05 were used for both the low-speed and high-speed process.

No friction is implemented between the supporter and the tube, while bilateral sticking contact is implemented between the tube and the puller. Latham & Cockcroft Normalized (*LCn*) damage model is activated in all simulations with a damage threshold of 0.36 according to literature for room temperature [12]. The definition of $LCn$ is given in the Eqn. 4:

$$LCn = \int^{\bar{\varepsilon}_f} \frac{\sigma_{max}}{\bar{\sigma}} d\bar{\varepsilon} \quad (4)$$

$\sigma_{max}$: maximum tensile stress, equal to the principal stress $\sigma_1$ in the axial direction

$\bar{\sigma}$: effective stress

$\bar{\epsilon}_f$: equivalent strain at which the fracture occurs

Pure Mg was chosen for the simulations for the tubes, and the data obtained from uniaxial tensile tests to failure before drawing, described above, were used to model the material by the Forge software, which uses the Hansel & Spittel flow stress law reported in Eqn. 5:

$$\sigma_f = A e^{m_1 T} \varepsilon^{m_2} \dot{\varepsilon}^{m_3} e^{\frac{m_4}{\varepsilon}} (1+\varepsilon)^{m_5 T} e^{m_7 \varepsilon} \dot{\varepsilon}^{m_8 T} T^{m_9} \quad (5)$$

The obtained non-zero coefficients are: $A$ = 210 MPa, $m_1$ = - 0.0009, $m_2$ = 0.0693441, $m_3$ = 0.022. All temperature-dependent coefficients are equal to zero, except $m_1$, which is very close to zero anyway, i.e. there is a negligible influence of temperature on the material properties.

## 3. RESULTS

### 3.1 Material characterization

The stress-strain graphs obtained from the uniaxial tensile tests are shown in Fig. 5(a).

As it can be seen, the ultimate tensile strength *UTS* values assume 40.87% higher values when the magnesium was subjected to the drawing process. In fact, the initial averaged $UTS_0$ is equal to 173.3 MPa ($\sigma$ = 2.55 MPa), lower than that measured after the cold deformation process $UTS_n$, equal to 244.12 MPa ($\sigma$ = 27.67 MPa), (T-Test, p-value < 0.05).

Furthermore, a large increase of 41% in the hardness of the sample is observed. In fact, in both cases the T-Test performed after checking the normality of the data confirmed a significant statistical difference (p-value < 0.05). This phenomenon can be attributed to work hardening of the material due to the plastic deformation (see Fig. 5(b)). These factors are not affected by the drawing speed $v$ (T-Test, p-value > 0.05).

Moreover, from an analysis of the microstructure of the drawn microtubes shown in Fig. 6, a twinned structure is always present.

### 3.2 Surface roughness, tube dimensions and cross-section circularity

After verifying the normality of the data, a paired T-Test showed that the surface quality of the microtubes improved compared with the starting condition (p-value < 0.05). A 34% reduction in the value of $Sa$ downstream the drawing process was found. The results are shown in Fig. 7(a). In any case, $Sa_n$ is not affected by the drawing speed $v$ (T-Test, p-value > 0.05).

The average measured value of the outer diameter at the outlet of the tube $D_{n-out}$ is equal to 754 μm ($\sigma$ = 2.62 μm) and is larger than the hole diameter of the die (740 μm, see Table 1). This means that the material undergoes springback as it exits the die. As expected, a microtube average wall thickening of 5.98% was observed due to hollow sinking drawing (paired T-Test, p-value < 0.05). The results are shown in Fig. 7(b).

In fact, the absence of an internal tool does not provide control of the internal lumen of the tube. This factor, added to the springback of Mg, produces a $R_{\%}$ value calculated according to Eqn. 1 equal to 6.44%, lower than the expected 11.34%. The drawing speed had no influence on the thickening of the microtube wall or the outer diameter achieved (T-Test, p-value > 0.05). The paired T-Tests were performed after verifying normality of the data. Comparing the cross-sectional area of the samples before drawing in Fig 2 (a) with that of the drawn samples in Fig 6, an improvement in circularity is observed. In fact, the circularity varies greatly between samples before drawing (see Fig 7 (c)). Subsequently, the passage through the die improved the circularity condition of the tube while also reducing its variability.

### 3.3 Drawing forces as monitoring factor

The graph shown in Fig. 8 represents as an example the trend of forces acquired by the load cell during the drawing process of two samples. The force signal increases in the initial drawing phase and then stabilize at a constant value that is maintained throughout the process. In this period, the force reaches values that vary depending on the drawing speed. In fact, it has been observed that the drawing force increases as $v$ increases (T-Test, p-value < 0.05) as shown in Fig. 7(d). From the force signals, it is possible to detect if instabilities have occurred during drawing, and thus associate changes in $F$ with defects/breakages in the material. In fact, the green signal in Fig. 8 represents the drawing force trend of a single sample, during which a displacement of the die within the setup occurred. This movement resulted in a change in force, which, however, stabilizes again in the following instants.

### 3.4 FE simulations results

Simulations showed that the damage suffered by pure Mg microtubes according to the Latham & Cockcroft Normalized damage model is below the threshold of 0.36. This means that the drawn tubes are safely far from their failure limit. Given that the tested reduction value is only 6%, the FE analyses suggest that larger $R_{\%}$ values could be used in this process, to obtain smaller diameters and thickness capillaries. It was observed that the value of *LCn* obtained as an output from the simulations in the inner region of the tube is higher than the outside one. In this case, the risk of failure is greater in the inner region of the tube compared to the outer region, consequently, the probability of encountering an internal crack is higher. Interestingly, the maximum value of $LCn_{\max}$ in the inner region slightly decreases as the drawing speed increases. In fact, *LCn* reaches high values in multiple areas at both speeds, even if critical areas are not extensive for a low drawing speed ($LCn_{\max}$ = 0.157 for $v$ = 50 mm/min) with respect to high speeds ($LCn_{max}$ = 0.148 for $v$ = 500 mm/min), (see Fig. 9). It is also noteworthy that the temperature increases in the tube due to an increased speed amounts to only about 5°C.

It can be seen in Fig. 7(b) and Fig. 7(d) that $Th_n$ and forces obtained from the simulations during the drawing process are of the same order of magnitude as those obtained experimentally.

## DISCUSSION

Mg tubular products are increasingly becoming relevant for medical applications but, due to its HCP structure, the drawing process can lead to several issues, such as poor ductility at room temperature, low finished product yield and high costs. Moreover, the drawing process becomes more challenging when working with thinwalled microcomponents due to dimensional effects.

In this study, the hollow sinking drawing method was used to obtain cold drawn Mg-based capillary structures. Changes from the initial state of the tubes in mechanical properties, surface roughness and wall thickness were observed, and the possible influence of process speed on these factors was investigated. Drawing forces were also examined as outputs. In addition, FE simulations were conducted to assess the risk level of magnesium microtube damage.

The results of the experiments are not dependent on the drawing speed used, except for the drawing forces. Probably, the selected range of *v*, imposed by the limits of the dynamometer used, is restricted and far from a real drawing speed. In fact, in real cases, the drawing velocity could be much higher in order to increase productivity.

Nevertheless, it has been observed that both the *UTS* and the microhardness of Mg increase by the 41% due to the work hardening imposed by the cold drawing process. This phenomenon reduces the ability of Mg to plastically deform, which means that numerous cold drawing and alternating annealing steps are required to maintain good formability of this material in order to achieve high cross-sectional area reductions. In fact, applying appropriate temperature and duration, annealing induces stress relief and grain growth necessary for enhanced formability and reduced risk of failure during the drawing process [17]. Furthermore, a twinned structure of the material was observed, which was already present in the samples before being drawn. At every stage of the drawing procedure, additional dislocations and twins can be introduced. The influx of defects may excessively embrittle the structure, compromising formability. On the other hand, doing more annealing process with higher temperature and time may cause grain growth and strength loss, with higher formability and lower probability of failure during drawing can be achieved [19]. The severe plastic deformation allows the formation of an ultrafine-grained structure in magnesium alloy tubes. This structural refinement leads to a substantial improvement in the mechanical properties, as well as a moderate enhancement in biocorrosion resistance [20].

Moreover, experiments showed an improvement in the surface quality of the as received material. The cold drawing process performed has improved the surface finish, hence an increase in corrosion resistance could be expected [18]. As reported in the study by Hanada et al. [21], machine oil, such as the one used in the present work, represents the best lubricant for the magnesium cold drawing process. In fact, machine oil allows an average surface roughness of 0.24 μm to be obtained. In addition, circularity of cross-section of the tube was improved by the drawing process. This first pass in the die can therefore be used to adjust the tube and to have a uniform cross-section, and thus a better stress distribution.

Also, this study showed that cold microdrawing using the hollow sinking strategy leads to a thickening of the wall, according to literature [10]. This occurs when using very small tubes, due to the absence of a mandrel inside, which is normally used in solid or liquid form for thickness control.

Force monitoring, which provides information on the status of the process such as anomalies, breakages or instabilities that may occur during the drawing, showed an increase of $F$ with increasing speed, due to the fact that the material is strain rate-dependent and from the presence of machine inertia.

FE simulations, finally demonstrated the low level of risk of magnesium microtube breakage using the proposed drawing speeds. Although it has been observed that this damage has a smaller magnitude when drawing at higher speeds, the difference is small and therefore this effect can be considered negligible. In fact, simulations show that the temperature increase during the process is only 5° C, not enough to soften the material. Moreover, it can be affirmed that the forces and thicknesses obtained through simulations align with experimental results. This means that the choice of keeping the same friction coefficients for both simulations returned outputs concordant to the experimental data. In fact, it was observed that larger values of $\mu$ and $\bar{\mu}$ returned higher force values than those measured experimentally. The coefficients, which define the flow stress law, were also chosen appropriately.

**CONCLUSIONS**

This study, provides an effective method for obtaining Mg-based thin-walled microtubes by means of cold drawing process with diameters smaller than one millimeter. Thus, this approach can be used for obtaining miniaturized magnesium devices for biomedical applications, where very small dimensions are required for the anatomical district of interest. The most relevant obtained results are listed below.

1. Cold drawing of magnesium is possible using the hollow sinking to achieve cross-sectional reductions up to approximately 6-7%.
2. Lubricating the outer surface of the tube with machine oil improves the finish when in contact with the die.
3. Plastic deformation leads to material hardening, increasing hardness and ultimate tensile strength by 41%, accompanied by the occurrence of mechanical twins.
4. Increasing the drawing speed by an order of magnitude, and thus the productivity of the process, does not seem to increase the level of material damage nor the temperature, which is quite remarkable in an industrialization perspective.
5. The model used for FE simulations returns values of forces and final wall thicknesses of microtubes in agreement with experimental data.

The biomedical research field is highly interested in magnesium device production due to its exceptional suitability for biocompatible and biodegradable applications. While this work serves as an initial step in obtaining tubular Mg-based microcomponents, further exploration is needed to understand the mechanical properties after multiple drawing passes and potential heat treatments for material crystalline structure restoration. This is the topic for further research. Furthermore, it is essential to study the corrosion rate in biological fluids, considering the extent of plastic deformation experienced.

## ACKNOWLEDGMENT

The authors thank Ertuğrul Kaya and Daniele Farioli of Politecnico di Milano for their invaluable support during this work.

## REFERENCES


[1] Li, N., and Zheng, Y., 2013, "Novel Magnesium Alloys Developed for Biomedical Application: A Review," *Journal of Materials Science and Technology,* **29**(6), pp. 489–502.

[2] Li, X. J., Xie, L., Pan, F. S., Wang, Y., Liu, H., Tang, Y. R., and Hutnik, C., 2018, "A feasibility study of using biodegradable magnesium alloy in glaucoma drainage device," *International Journal of Ophthalmology,* **11**(1), pp. 135–142.

[3] Wang, J., Giridharan, V., Shanov, V., Xu, Z., Collins, B., White, L., Jang, Y., Sankar, J., Huang, N., and Yun, Y., 2014, "Flow-induced corrosion behavior of absorbable magnesium-based stents," *Acta Biomaterialia*.

[4] Sezer, N., Evis, Z., Kayhan, S., Tahmasebifar, A., and Koc¸, M., 2018, "Review of magnesium-based biomaterials and their applications," *Journal of Magnesium and Alloys,* **6**(1), pp. 23–43.

[5] Ramalingam, V. V., Ramasamy, P., Kovukkal, M. D., and Myilsamy, G., 2020, "Research and Development in Magnesium Alloys for Industrial and Biomedical Applications: A Review," *Metals and Materials International,* **26**(4), pp. 409–430.

[6] Lopes, V., Puga, H., Gomes, I. V., Peixinho, N., Teixeira, J. C., and Barbosa, J., 2022, "Magnesium stents manufacturing: Experimental application of a novel hybrid thin-walled investment casting approach," *Journal of Materials Processing Technology,* **299**(July 2021).

[7] Wang, W., Nune, K. C., Tan, L., Zhang, N., Dong, J., Yan, J., Misra, R. D., and Yang, K., 2019, "Bone regeneration of hollow tubular magnesium-strontium scaffolds in critical-size segmental defects: Effect of surface coatings," *Materials Science and Engineering C,* **100**(February), pp. 297–307.

[8] Bella, P., Kan, M., Ridzon, M., and Mojzis, M., 2020, "Simulation of two hollow sinking passes in one tool," *Procedia Manufacturing,* **50**, pp. 407– 410.

[9] Furushima, T., and Manabe, K., 2018, "Large reduction die-less mandrel drawing of magnesium alloy micro-tubes," *CIRP Annals,* **67**(1), pp. 309–312.

[10] Yoshida, K., and Koiwa, A., 2011, "Cold Drawing of Magnesium Alloy Tubes for Medical," *Journal of Solid Mechanics and Materials Engineering,* **5**(12),

pp. 1071–1078.

[11] Yan, Z., Fang, M., Lian, Z., Zhang, Z., Zhu, J., Zhang, G., and Wang, Y., 2019, "Research on AZ80 + 0.4%ce (wt %) ultra-thin-walled tubes of magnesium alloys: The forming process, microstructure evolution and mechanical properties," *Metals,* **9**(5), pp. 1–15.

[12] Kim, S. W., and Lee, Y. S., 2014, "Comparative study on failure prediction in warm forming processes of Mg alloy sheet by the FEM and ductile fracture criteria," *Metallurgical and Materials Transactions B: Process Metallurgy and Materials Processing Science,* **45**(2), pp. 445–453.

[13] Zhang, Z., Yan, Z., Du, Y., Zhang, G., Zhu, J., Ren, L., and Wang, Y., 2018, "Hot deformation behavior of homogenized Mg-13.5Gd-3.2Y-2.3Zn-0.5Zr alloy via hot compression tests," *Materials,* **11**(11), pp. 1–19.

[14] Zhang, G., Zhang, Z., Li, X., Yan, Z., Che, X., Yu, J., and Meng, Y., 2019, "Effects of repetitive upsetting-extrusion parameters on microstructure and texture evolution of Mg–Gd–Y–Zn–Zr alloy," *Journal of Alloys and Compounds,* **790**, pp. 48–57.

[15] Bruschi, S., Altan, T., Banabic, D., Bariani, P. F., Brosius, A., Cao, J., Ghiotti, A., Khraisheh, M., Merklein, M., and Tekkaya, A. E., 2014, "Testing and modelling of material behaviour and formability in sheet metal forming," *CIRP Annals - Manufacturing Technology,* **63**(2), pp. 727–749.

[16] Wang, L., Fang, G., Qian, L., Leeflang, S., Duszczyk, J., and Zhou, J., 2014, "Forming of magnesium alloy microtubes in the fabrication of biodegradable stents," *Progress in Natural Science: Materials International,* **24**(5), pp. 500–506.

[17] Dodyim, N., Yoshida, K., Murata, T., and Kobayashi, Y., 2020, "Drawing of magnesium fine wire and medical application of drawn wire," *Procedia Manufacturing,* **50**(2019), pp. 271–275.

[18] Nguyen, T. L., Blanquet, A., Staiger, M. P., Dias, G. J., and Woodfield, T. B., 2012, "On the role of surface roughness in the corrosion of pure magnesium in vitro," *Journal of Biomedical Materials Research - Part B Applied Biomaterials,* **100 B**(5), pp. 1310–1318.

[19] Amani, S., and Faraji, G., 2019, "Processing and Properties of Biodegradable Magnesium Microtubes for Using as Vascular Stents: A Brief Review," *Metals and Materials International,* **25**(5), pp. 1341–1359.

[20] Hwang, Y., Huang, S., and Huang, Y., 2013, "Study of seamless tube extrusion of SiCp-reinforced AZ61 magnesium alloy composites," *International Journal of Advanced Manufacturing Technology,* **68**(5-8), pp. 1361–1370.

[21] Hanada, K., Matsuzaki, K., Huang, X., and Chino, Y., 2013, "Fabrication of Mg alloy tubes for biodegradable stent application," *Materials Science and Engineering C,* **33**(8), pp. 4746–4750.

## Figure Captions List

Fig. 8 Drawing force trend as a function of displacement, with $v$ = 500 mm/min. The signals were acquired from the load cell during drawing, and refer to two example samples (squares signal and circles signal).

Fig. 9 FE simulations results. *LCn* contour plot for different drawing velocities in the inner region of the microtube.

**Table Caption List**

Table 1 Geometrical characteristics of the die as $D_{die}$: die exit diameter; $2\alpha$: approach angle; $L_b$: bearing length.

Table 2 Drawing test conditions and samples. Level 1 refers to the lower level of speed (-), while Level 2 refers to the higher level of speed (+).

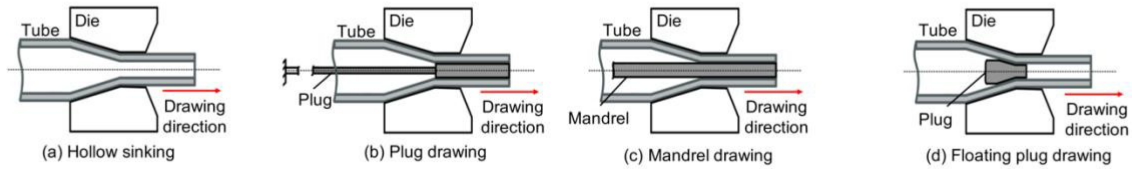


Figure 1 Commonly used drawing techniques

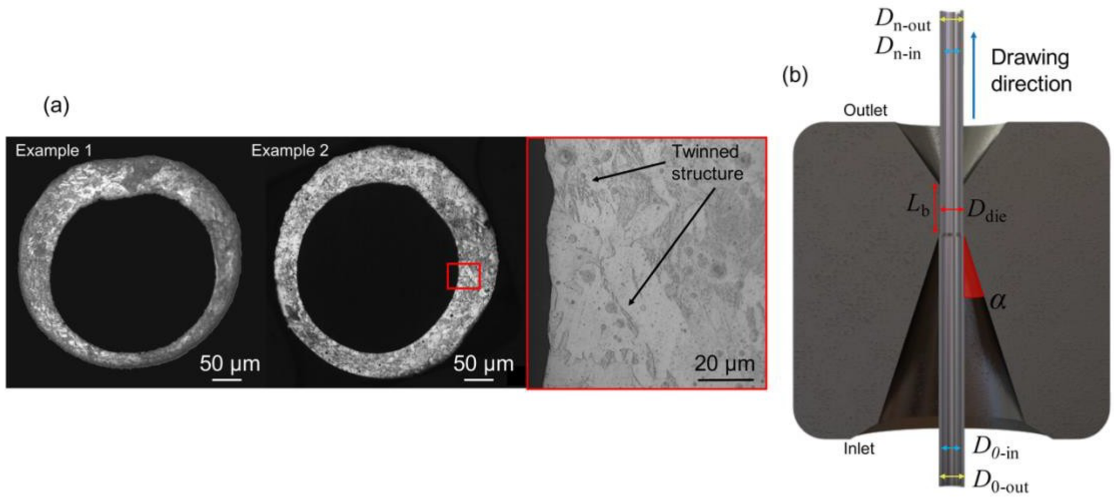


Figure 2 (a) Cross-section examples and microstructure of the as received magnesium tube. (b) Hollow sinking drawing process.

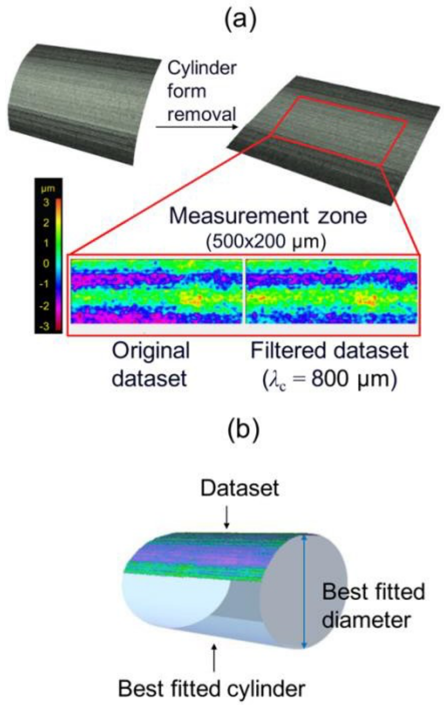


Figure 3 (a) Surface roughness measurement of the region of interest after cylinder form removal. (b) Tube outer diameter measurement.

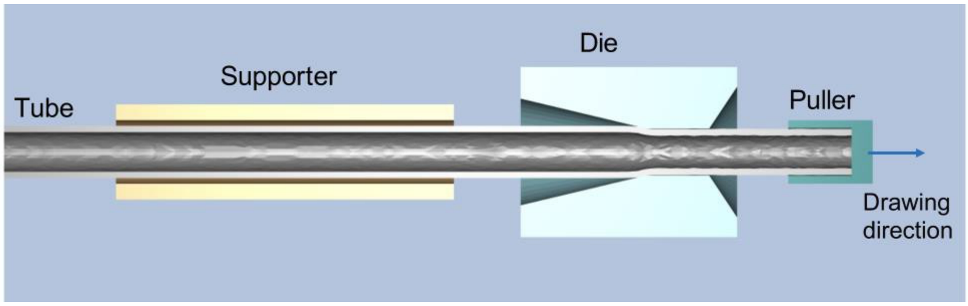

Figure 4 FE implemented setup

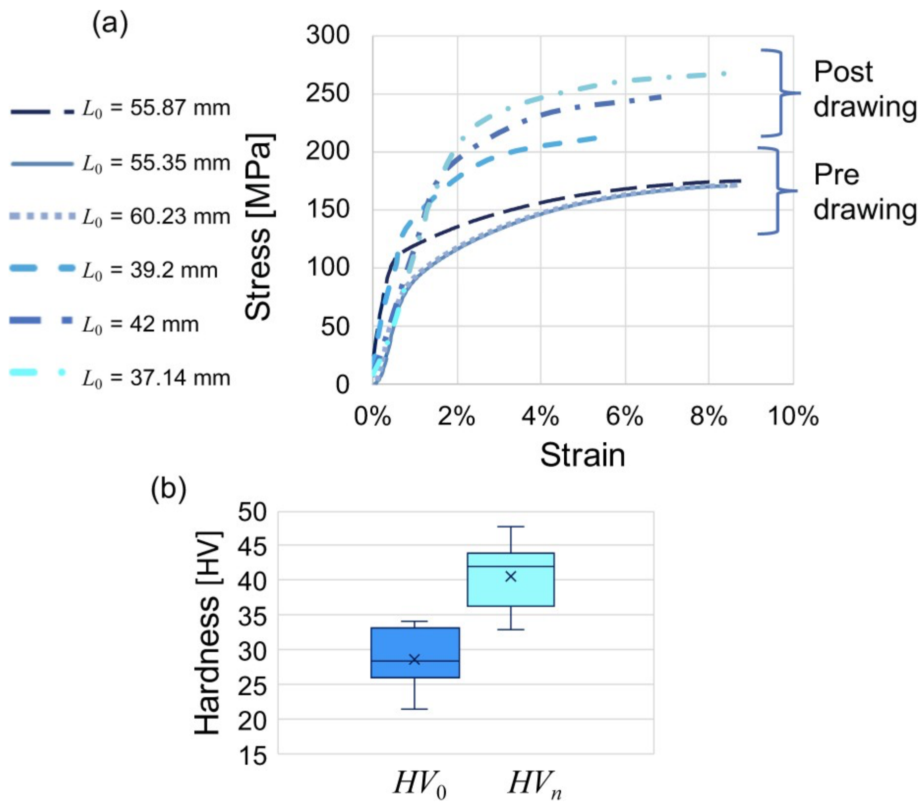


Figure 5 (a) Stress-Strain deformation curves obtained before and after drawing. The legend shows the initial stretch of the samples $L_0$, which is the distance between the machine grips before the tensile tests. (b) Microhardness box plots results. $H_0$: initial microhardness; $H_n$: final microhardness.

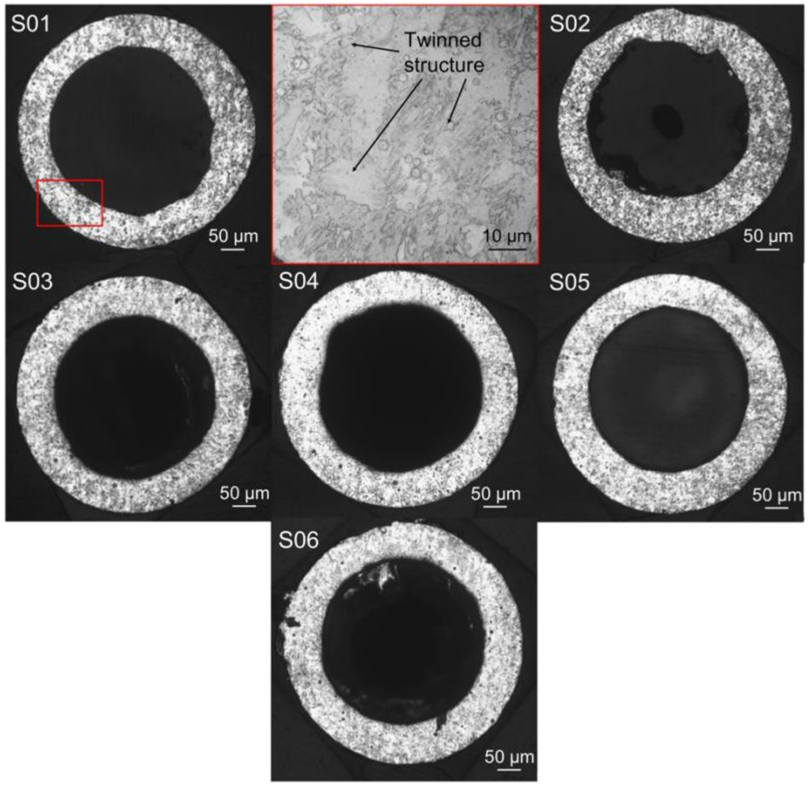


Figure 6 Drawn microtubes cross-sections and their microstructure

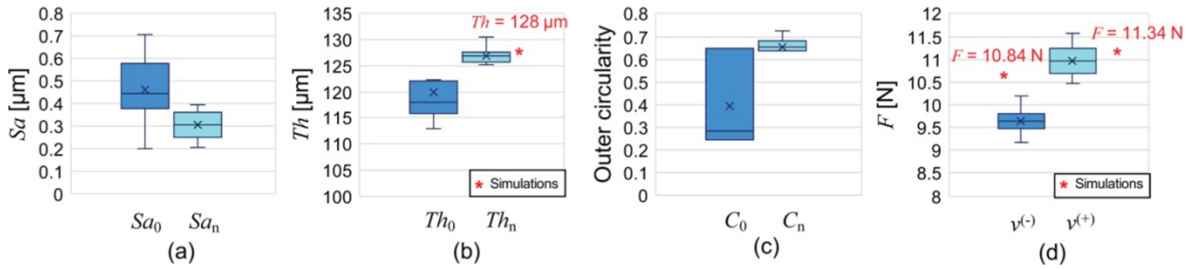


Figure 7 (a) Sa box plots. $Sa_0$: initial surface roughness; $Sa_n$: final surface roughness. (b) *Th* box plots. $Th_0$: initial thickness; $Th_n$: final thickness. The asterisk in the graph shows the value of *Th* obtained by FE simulations (c) Outer circularity box plots $C_0$ initial outer circularity; $C_n$ final outer circularity. (d) Forces box plots. The asterisks in the graph show of the values of forces obtained by FE simulations.

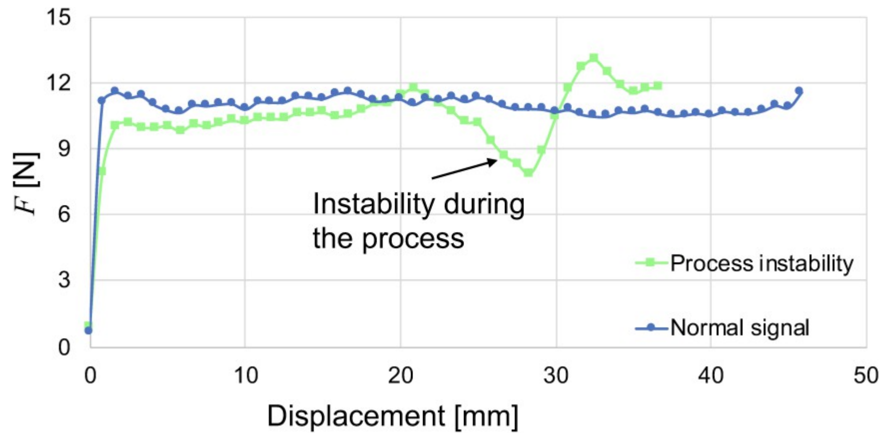


Figure 8 Drawing force trend as a function of displacement, with $v$ = 500 mm/min. The signals were acquired from the load cell during drawing, and refer to two example samples (green signal and blue signal).

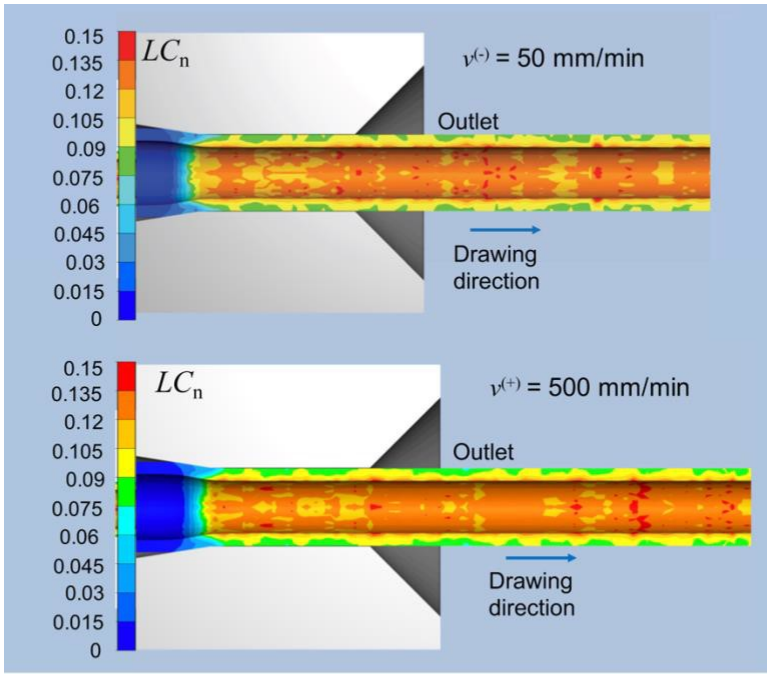


Figure 9 FE simulations results. *LCn* contour plot for different drawing velocities in the inner region of the microtube.

***Table 1*** Geometrical characteristics of the die as $D_{die}$: die exit diameter; $2\alpha$: approach angle; $L_b$: bearing length.

| $D_{die}$ [μm] | $2\alpha$ [deg] | $L_b$ [mm] |
|---|---|---|
| 740 | 18 | 1.5 |

**Table 2** Drawing test conditions and samples. Level 1 refers to the lower level of speed (-), while Level 2 refers to the higher level of speed (+).

| Testscheme | Level 1 (-) | Level 2 (+) |
|---|---|---|
| *v* [mm/min] | 50 | 500 |
| SAMPLE | S01, S03, S05 | S02, S04, S06 |